

Extreme Learning Machine for Biomedical Image Classification: A Multi-Case Study

Francesco Mercaldo^{1*}, Luca Brunese¹, Antonella Santone¹, Fabio Martinelli², Mario Cesarelli³

¹University of Molise, Campobasso, Italy

²Institute for Informatics and Telematics, National Research Council of Italy, Pisa, Italy

³University of Sannio, Benevento, Italy

Abstract

In the current realm of biomedical image classification, the predominant choice remains deep learning networks, particularly convolutional neural network (CNN) models. However, deep learning suffers from a notable drawback in terms of its high training cost, mainly due to intricate data models. A recent alternative, known as the Extreme Learning Machine (ELM), has emerged as a promising solution. Empirical investigations have indicated that ELM can offer satisfactory predictive performance for a wide array of classification tasks, while significantly reducing training costs when compared to deep learning networks trained using back propagation. This research paper introduces a methodology designed to evaluate the suitability of employing the Extreme Learning Machine for biomedical classification tasks. Our study encompasses binary and multiclass classification across four distinct scenarios, involving the analysis of biomedical images obtained from both dermatoscopes and blood cell microscopes. The findings underscore the effectiveness of the Extreme Learning Machine, showcasing its successful utilization in the classification of biomedical images.

Received on 23 December 2023; accepted on 17 March 2024; published on 25 March 2024

Keywords: Extreme Learning Machine, ELM, Biomedical Image, Classification, Machine Learning.

Copyright © 2024 F. Mercaldo *et al.*, licensed to EAI. This is an open access article distributed under the terms of the Creative Commons Attribution license (<http://creativecommons.org/licenses/by/3.0/>), which permits unlimited use, distribution and reproduction in any medium so long as the original work is properly cited.

doi:10.4108/eetpht.10.5542

1. Introduction

In the realm of biomedical image classification, deep learning networks, specifically convolutional neural network (CNN) models, are the current favorite [1]. These networks utilize the backpropagation algorithm, introduced by Rumelhart et al., which iteratively propagates errors from output nodes to input nodes, providing a fundamental gradient-based method for parameter optimization. However, deep learning encounters challenges like slow convergence and susceptibility to local minima. To address these challenges, researchers have explored various techniques to enhance the efficiency and effectiveness of training feedforward neural networks, including second-order optimization techniques [2], subset selection methods [3], and global optimization strategies [4]. Many of these methods, despite their potential to expedite training or improve generalization compared to backpropagation, do not guarantee globally optimal solutions.

Recently, a novel approach known as the Extreme Learning Machine (ELM) has gained prominence as a means to train

Single Hidden Layer Feedforward Neural Networks (SLFNs) [5]. ELM introduces hidden nodes in a random manner and keeps them fixed without iterative adjustments. Importantly, these hidden nodes in the ELM architecture do not need to adhere to a neuron-like structure. The only parameters subject to learning are the connections (i.e., weights) linking the hidden layer to the output layer. This makes ELM essentially a linear model in terms of its parameters, simplifying the process to solving a linear system. Compared to traditional approaches for training feedforward neural networks, ELM exhibits remarkable efficiency and tends to converge toward a global optimum. Theoretical analyses have demonstrated that, even with randomly generated hidden nodes, ELM retains the universal approximation capability inherent in SLFNs [6, 7].

When employing common activation functions, ELM can approach the optimal generalization limit observed in traditional feedforward neural networks, where all parameters undergo learning [8, 9]. Empirical evidence supports the efficiency and generalization performance of ELM compared to traditional Feedforward Neural Network (FNN) algorithms across various domains [7, 10]. Notably, ELM exhibits significantly higher efficiency

*Corresponding author. Email: francesco.mercaldo@unimol.it

compared to Support Vector Machines (SVM) [11], Least Square Support Vector Machines [12], and other advanced algorithms. Empirical investigations have shown that ELM's generalization capabilities are equivalent to or even superior to those of SVMs and their variants [7, 13, 14]. Comprehensive comparisons between ELM and SVM can be found in [15] and [16].

1.1. Recent Developments in Medical Image Classification

In recent years, there has been an increased utilization of feedforward neural networks in classifying medical images [17–20]. Deep learning, a subset of machine learning [21–23], has gained attention for its ability to create a hierarchy of features and distinguish lower-level attributes from higher-level ones. Image classification, a crucial task in computer vision, involves assigning images to predefined categories. Deep learning techniques, including multilayer nonlinear data processing, classification, feature selection, transformation, and structural identification, have been deployed to address this challenge. Among these techniques, the Convolutional Neural Network (CNN) has become the primary framework for recognizing, classifying, and analyzing various medical images.

In the past, Support Vector Machines (SVM) were the conventional choice for biomedical image classification [24]. However, SVM has limitations, including time-consuming feature extraction from images and lower performance compared to various alternatives. Therefore, the trend in biomedical image classification has shifted towards advocating for deep learning-based approaches [24].

For instance, Ali et al. employed supervised machine learning techniques to achieve high classification accuracies on cervical cancer cell datasets [25]. Urushibara et al. demonstrated the diagnostic performance of deep learning in cervical cancer using MRI images [26]. Mohsen et al. utilized deep neural networks for brain MRI segmentation and achieved promising results [27]. Brain cancer grade detection was explored by Zia et al., employing deep learning alongside other techniques [28].

However, deep learning has its limitations, including the need for a substantial amount of data and resource-intensive training procedures, necessitating expensive hardware [29].

1.2. Investigating ELM in Biomedical Image Classification

Given these considerations, this paper investigates the potential of using ELM in biomedical image classification. The study spans two biomedical domains: dermatoscopic and blood cell microscope images, resulting in four distinct case studies encompassing both binary and multiclass classification scenarios. These case studies collectively demonstrate the feasibility of employing ELM in biomedical image classification.

Furthermore, this study conducts a comparative analysis between the ELM model and the established AlexNet model [30], widely used in biomedical image classification [31–33].

To the best of our knowledge, this paper represents the first exploration of ELM's application in biomedical image classification.

1.3. Paper Structure

The paper is structured as follows: the next section introduces the proposed approach for biomedical image classification using ELM. Section 3 outlines the four distinct case studies conducted in the domains of dermatoscopic and blood cell microscope images. Finally, the concluding section summarizes the findings and outlines future research prospects.

2. The Method

In this section, we provide an extensive explanation of our methodology for employing extreme learning machines in the classification of biomedical images.

Our approach consists of two main phases. The initial phase, referred to as the 'Training' phase (as depicted in Figure 1), focuses on constructing a model using an extreme learning machine. The subsequent phase, known as the 'Testing' phase (illustrated in Figure 2), revolves around evaluating the classification performance of the ELM model created during the training phase.

The initial step, as illustrated in Figure 1, involves the utilization of the 'Biomedical Image Repository.' It is essential to highlight that ELM belongs to the realm of machine learning models, emphasizing their reliance on data. This underscores the critical need for a substantial volume of unbiased and accurately labeled data, which is particularly significant when dealing with biomedical images, as demonstrated in our case studies.

The subsequent phase focuses on converting images, especially those originally not in grayscale, into grayscale format. This conversion is motivated by the idea that color may not be essential for pathology detection in the biomedical context, a concept that we will explore more comprehensively in the case studies. Additionally, this step contributes to reducing the time required for model development.

After biomedical images are transformed into grayscale, they undergo resizing to dimensions of 28 pixels in width and 28 pixels in height. Each pixel from these grayscale images is then organized as an element within a vector. Consequently, for each image, a vector comprising $28 \times 28 = 784$ pixels is generated.

Following this transformation, which converts the images into numerical vectors, the data is prepared for input into the 'ELM network.'

To effectively train the ELM model, it is crucial to split the previously acquired dataset into two separate sets: one designated for training and the other for testing.

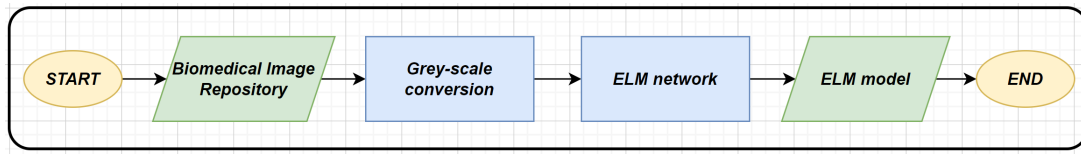


Figure 1. The model training step.

We utilize a 'OneHotEncoder' function to convert our target values into one-hot encoding and employ the 'MinMaxScaler' function to normalize the features, ensuring they fall within the (0, 1) range.

After normalizing the features and converting the targets to one-hot encoding, the initialization of the ELM network entails specifying the following elements:

1. The dimensions of the input layer, which align with the number of input features (in our instance, 28x28).
2. The quantity of hidden neurons (we employ 1000 in our configuration).
3. The weights connecting the input to the hidden layer, which are randomly sampled from a Gaussian distribution.
4. The activation function applied to the hidden layer (we employ the Rectified Linear Unit (ReLU) function).

The objective of the ELM network is to build the 'ELM Model.'

Figure 2 illustrates the Testing phase, designed to assess the performance of the 'ELM model' established in the preceding phase for biomedical image classification.

To evaluate the performance of the ELM model, we employ a dataset of images that were not included in the training phase. This entails selecting a biomedical image of interest, which may come from sources such as a dermatoscope or a microscope. The chosen image is converted into grayscale, resized to 28x28 dimensions, and subsequently fed into the 'ELM model.' This procedure leads to the model generating an output label that corresponds to the image, effectively accomplishing the classification task.

3. Experimental Analysis

To gauge the effectiveness of the models we put forth, we calculate four separate metrics: Precision, Recall, F-Measure, and Accuracy.

In a testing context, *Precision* indicates the proportion of true negatives relative to all actual negative cases. It's mathematically defined as:

$$Precision = \frac{tn}{tn + fp}$$

where tn are true negatives and fp signifies false positives.

Recall within the classification context denotes the fraction of true positive instances among all the actual positive cases.

It can be expressed as:

$$Recall = \frac{tp}{tp + fn}$$

where tp stands for true positives and fn corresponds to false negatives.

The *F-Measure* is a combined metric that considers both specificity and sensitivity:

$$F-Measure = 2 \times \frac{Precision \times Recall}{Precision + Recall}$$

Accuracy, conversely, offers a holistic evaluation encompassing both random and systematic observational errors. It necessitates the attainment of both high precision and high recall to attain elevated accuracy.:

$$Accuracy = \frac{tn + tp}{tn + tp + fn + fp}$$

These metrics have been computed to assess the ELM model's performance in the context of four specific case studies. Additionally, as mentioned earlier in the introduction, we conduct a comparative analysis between the ELM model and the AlexNet model. AlexNet, which features a convolutional neural network architecture, consists of a total of eight layers. The initial five layers are convolutional, some followed by max-pooling layers, while the last three layers are fully connected. It incorporates the non-saturating ReLU activation function, which has demonstrated superior training performance compared to tanh and sigmoid functions, as demonstrated in [30]. The AlexNet model is trained for a single epoch using images resized to dimensions of 224x224 with 3 RGB channels.

For the experimental setup, we employed a computer equipped with an 8th Generation Intel i7 CPU and 16GB of RAM, running the experiments in a Windows 10 environment with Windows Subsystem for Linux.

Both the ELM and AlexNet models were developed using Python version 3.6.9. In particular, for implementing the AlexNet model, we utilized Tensorflow library version 2.4.4, as detailed in [34].

3.1. The Datasets

To assess the suitability of ELM for tasks related to biomedical image classification, we utilize two separate datasets sourced from the MedMNIST repository, which can

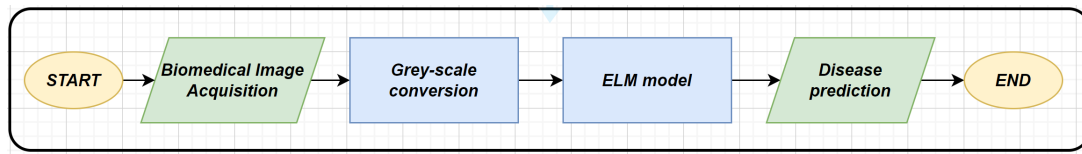


Figure 2. The model testing step.

be accessed at ¹, as detailed in [35]. This repository offers a standardized collection of biomedical images captured from various organs and using different imaging instruments.

Each image undergoes preprocessing to conform to a 2D format with dimensions of 28 x 28 pixels and is associated with its corresponding classification label. To be more specific, our dataset consists of biomedical data obtained from two equipment categories: dermatoscopes and blood cell microscopes. This deliberate selection highlights the versatility of ELM in addressing various biomedical image classification tasks, including both multiclass and binary scenarios.

Our analysis begins with the DermaMNIST dataset, which is a subset derived from the HAM10000 repository, as explained in [36, 37]. This dataset comprises a diverse collection of dermatoscopic images featuring common pigmented skin lesions. In total, the DermaMNIST dataset includes 10,015 dermatoscopic images, with 8,010 designated for training and the remaining 2,005 for testing purposes. These images are categorized into 7 distinct disease categories, maintaining an 80:20 ratio between the training and testing sets. The original source images, initially sized at 3x600x450 pixels, are resized to dimensions of 3x28x28, resulting in each image having dimensions of 28x28 pixels with 3 RGB channels.

The DermaMNIST dataset encompasses the following multiclass classification categories, established to distinguish between various dermal diseases:

- Label 0: Actinic keratoses and intraepithelial carcinoma.
- Label 1: Basal cell carcinoma.
- Label 2: Benign keratosis-like lesions.
- Label 3: Dermatofibroma.
- Label 4: Melanoma.
- Label 5: Melanocytic nevi.
- Label 6: Vascular lesions.

For binary classification with the DermaMNIST dataset, the following labels are considered:

- Label 0: Actinic keratoses and intraepithelial carcinoma, basal cell carcinoma, benign keratosis-like lesions, dermatofibroma, melanocytic nevi, and vascular lesions.
- Label 1: Melanoma (related to the detection of melanoma disease).

Let us now turn our attention to the BloodMNIST dataset, which, much like the DermaMNIST dataset, forms part of the MedMNIST collection. The BloodMNIST dataset is derived from a dataset mentioned in [38]. This source dataset comprises individual normal blood cells obtained from individuals who were free from any infection, hematologic or oncologic diseases, and had not undergone any pharmacologic treatment at the time of blood sampling. The BloodMNIST dataset consists of a total of 17,092 images, with 13,671 allocated for model training and the remaining 3,412 for model testing. The dataset is categorized into 8 classes, with an 80:20 split between the training and testing sets. The original source images, initially sized at 3x360x363 pixels, undergo center-cropping to dimensions of 3x200x200 pixels before being resized to 3x28x28 dimensions. As a result, the images have dimensions of 28x28 pixels, with each pixel represented in three RGB channels.

The BloodMNIST dataset comprises multiclass classification labels, with a primary focus on the identification of blood cell types:

- Label 0: Basophil.
- Label 1: Eosinophil.
- Label 2: Erythroblast.
- Label 3: Immature granulocytes (including myelocytes, metamyelocytes, and promyelocytes).
- Label 4: Lymphocyte.
- Label 5: Monocyte.
- Label 6: Neutrophil.
- Label 7: Platelet.

For binary classification with the BloodMNIST dataset, the following labels are employed:

- Label 0: Basophil, eosinophil, erythroblast, immature granulocytes, lymphocyte, monocyte, and neutrophil cells.

¹<https://medmnist.com/>

Table 1. DermaMINST binary classification results.

Model	Precision	Recall	F-Measure	Accuracy	Time
ELM	0.843	0.872	0.854	0.872	0:00:33
AlexNet	0.343	0.343	0.320	0.343	0:13:13

- Label 1: Platelets.

The goal is to predict whether a microscopic blood image contains platelets or other types of blood cells.

3.2. Binary Classification Results

In this section, we present the results obtained from our binary classification experiments involving both the DermaMNIST and BloodMNIST datasets.

To clarify, our initial binary model focuses on melanoma detection. In this context, we represent $T_{detection}$ as a label set $\{(M_{detection}, l_{detection})\}$, where each $M_{detection}$ corresponds to a respective $l_{detection} \in \{0, 1\}$. Here, the value 1 indicates melanoma, while the value 0 represents other pathologies, including actinic keratoses, intraepithelial carcinoma, basal cell carcinoma, benign keratosis-like lesions, dermatofibroma, melanocytic nevi, and vascular lesions.

We construct a numerical feature vector, denoted as $F \in \mathbb{R}^y$, where y represents the number of features used during the learning phase ($y = 784$). Notably, for each 28x28 grayscale image under consideration, each pixel is treated as an individual feature.

Table 1 displays the classification results obtained from the binary classification process applied to the DermaMNIST dataset.

Table 1 demonstrates the superior performance of the ELM model over AlexNet. To be precise, the ELM model attains an accuracy of 0.872, while the AlexNet model achieves an accuracy of 0.343. Additionally, the training time for the ELM model is 33 seconds, whereas the AlexNet model demands over 13 minutes.

Figure 3 exhibits the associated confusion matrix for the binary classification of DermaMNIST with the ELM model.

The confusion matrix indicates that the ELM model accurately classifies 41 images as melanoma and 1709 images as other dermal pathologies.

Moving on, let's delve into the classification process and results achieved in binary classification using the BloodMNIST dataset. This second case study centers around platelet detection. In this context, we denote $T_{detection}$ as a label set $(M_{detection}, l_{detection})$, where each $M_{detection}$ label is associated with a respective $l_{detection}$ value $\in \{0, 1\}$. Here, the value 1 represents platelets, while the value 0 corresponds to other blood cell types, including basophil, eosinophil, erythroblast, immature granulocyte, lymphocyte, monocyte, and neutrophil.

Table 2 presents the outcomes derived from the binary classification conducted using the BloodMNIST dataset.

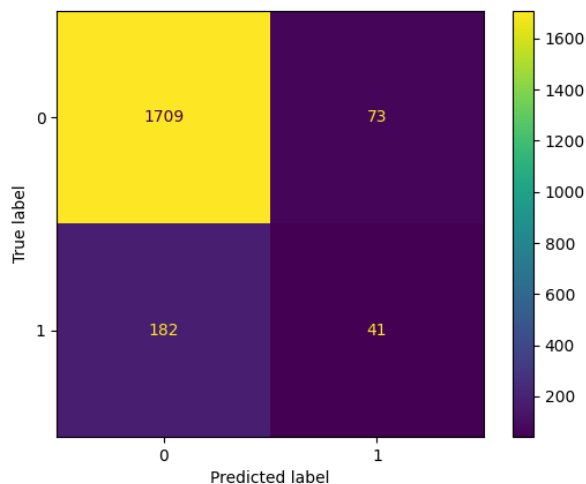

Figure 3. The DermaMINST binary classification confusion matrix.

Table 2. BloodMINST binary classification results.

Model	Precision	Recall	F-Measure	Accuracy	Time
ELM	0.997	0.997	0.997	0.997	0:00:28.73
AlexNet	0.991	0.991	0.990	0.991	0:18:45.48

The findings provided in Table 2 emphasize the strong performance of both the ELM and AlexNet models. Notably, the ELM classifier achieves an outstanding accuracy of 0.997, while the AlexNet model achieves an accuracy of 0.991. These outcomes underscore the ELM model's consistently slightly superior performance compared to AlexNet.

In terms of time efficiency, the ELM model concludes its training and testing processes in just 28 seconds, whereas the corresponding timeframe for the AlexNet model extends to 18 minutes and 45 seconds.

Figure 4 visually represents the confusion matrix for the binary classification of BloodMNIST, utilizing the ELM model.

Upon examining the confusion matrix depicted in Figure 4, it becomes evident that a total of 464 platelets and 2940 blood microscopic images representing other cell types are accurately classified.

3.3. Multiclass Classification Results

Now, let us explore the description of the classification process and the results obtained from multiclass classification using both the DermaMNIST and BloodMNIST datasets.

In this third case study, we focus on classifying different dermal pathologies using the DermaMNIST dataset. To achieve this, we utilize $T_{detection}$ as a set of labels $(M_{detection}, l_{detection})$, where each $M_{detection}$ label is associated with a corresponding $l_{detection}$ value $\in \{0, 1, 2, 3, 4, 5\}$.

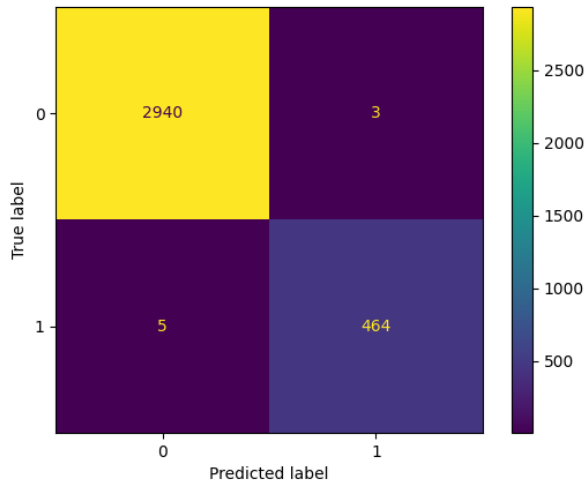


Figure 4. The BloodMINST binary classification confusion matrix.

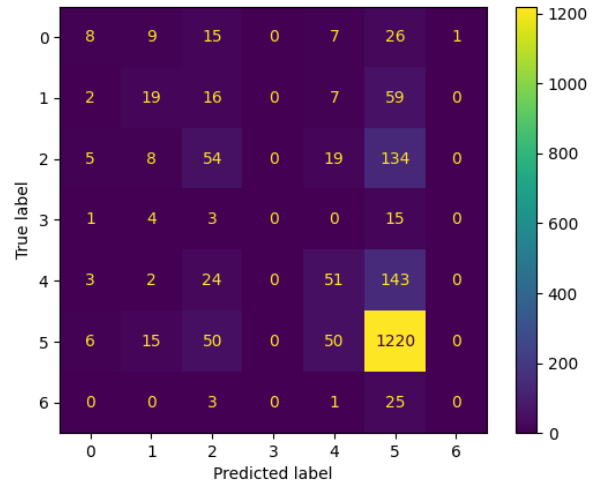


Figure 5. The DermaMINST multiclass classification confusion matrix.

Table 3. DermaMINST multiclass classification results.

Model	Precision	Recall	F-Measure	Accuracy	Time (sec)
ELM	0.608	0.674	0.631	0.674	0:00:23.21
AlexNet	0.655	0.317	0.425	0.668	0:26:00.99

Table 4. BloodMINST multiclass classification results.

Model	Precision	Recall	F-Measure	Accuracy	Time (sec)
ELM	0.700	0.702	0.696	0.702	0:00:39.21
AlexNet	0.984	0.073	0.134	0.269	0:26:00.99

6, 7. Specifically, labels 0 to 6 correspond to actinic keratoses and intraepithelial carcinoma, basal cell carcinoma, benign keratosis-like lesions, dermatofibroma, melanoma, melanocytic nevi, and vascular lesions, respectively.

Table 3 presents the results achieved in the multiclass classification of DermaMNIST.

The classification results presented in Table 3 reveal that the ELM model shows a slightly enhanced performance, achieving an accuracy of 0.674, as compared to the AlexNet model, which achieves an accuracy of 0.668. In terms of computational time, the ELM model finishes both training and testing in 23 seconds, whereas the same tasks necessitate the AlexNet model to run for 26 minutes

Figure 5 additionally presents the confusion matrix for the multiclass classification of DermaMNIST with the ELM model.

An analysis of the confusion matrix presented in Figure 5 reveals that a significant portion of dermal images is correctly classified into their respective classes, providing strong evidence of the ELM model’s efficacy.

The fourth and final case study introduced here focuses on multiclass classification using the BloodMNIST dataset. In this scenario, the objective is to differentiate between various blood cell types. To accomplish this, we define $T_{detection}$ as a set of labels $(M_{detection}, l_{detection})$, where each $M_{detection}$ label corresponds to a $l_{detection}$ value $\in \{0, 1, 2, 3, 4, 5, 6, 7\}$. Specifically, label values ranging from 0 to 7 correspond

to basophil, eosinophil, erythroblast, immature granulocytes, lymphocyte, monocyte, neutrophil, and platelet, respectively.

Table 4 presents the outcomes associated with the fourth case study, which is the multiclass classification of BloodMNIST.

The outcomes presented in Table 4 illustrate that the ELM model attains an accuracy of 0.702, whereas the AlexNet model reaches an accuracy of 0.269. Concerning computational time, the ELM model completes both the training and testing procedures in 39 seconds, whereas the AlexNet model requires 26 seconds.

Figure 6 further provides a visualization of the confusion matrix for the multiclass classification of BloodMNIST.

In the context of multiclass classification using BloodMNIST, it’s evident that a significant portion of instances is correctly categorized into their respective cell classes, affirming the effectiveness of ELM in identifying blood cells.

Upon examining the experimental results from the four case studies, it becomes evident that the ELM model consistently outperforms the AlexNet network in terms of accuracy in all scenarios. Additionally, this improved performance is accompanied by significantly reduced durations for both model training and testing phases.

4. Conclusion and Future Work

ELM represents an emerging paradigm capable of constructing predictive models that achieve comparable, if not

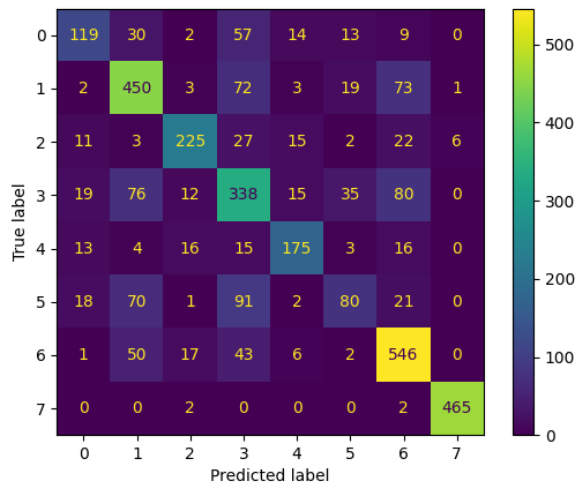


Figure 6. The BloodMINST multiclass classification confusion matrix.

superior performance to CNNs in significantly shorter timeframes. This study explores the potential of utilizing ELM for biomedical image classification tasks, an area historically dominated by deep learning, particularly CNNs. We present four distinct case studies: the first one employs the DermaMNIST dataset for binary classification, the second uses the BloodMNIST dataset for binary classification, the third employs the DermaMNIST dataset for multiclass classification, and the fourth involves the BloodMNIST dataset for multiclass classification. Across all four case studies, ELM consistently outperforms the widely-used AlexNet model, a prevalent deep learning architecture in biomedical image classification.

In our future research endeavors, we envision expanding our experiments to include biomedical images obtained through alternative imaging systems. While this study primarily focuses on images captured with dermoscopes and blood cell microscopes, our upcoming work will incorporate imagery from systems such as optical coherence tomography and computed tomography.

Acknowledgment

This work has been partially supported by EU DUCA, EU CyberSecPro, SYNAPSE, PTR 22-24 P2.01 (Cybersecurity) and SERICS (PE00000014) under the MUR National Recovery and Resilience Plan funded by the EU - NextGenerationEU projects.

References

[1] RUMELHART, D.E., HINTON, G.E. and WILLIAMS, R.J. (1986) Learning representations by back-propagating errors. *nature* **323**(6088): 533–536.

[2] HAGAN, M.T. and MENHAJ, M.B. (1994) Training feedforward networks with the marquardt algorithm. *IEEE transactions on Neural Networks* **5**(6): 989–993.

[3] CHEN, S., COWAN, C. and GRANT, P. (1991) Orthogonal least squares learning algorithm for radial. *IEEE Transactions on neural networks* **2**(2): 303.

[4] URGEN BRANKE, J. (1995) Evolutionary algorithms for neural network design and training. In *Proceedings of the 1st Nordic Workshop on Genetic Algorithms and its Applications* (Citeseer).

[5] HUANG, G., HUANG, G.B., SONG, S. and YOU, K. (2015) Trends in extreme learning machines: A review. *Neural Networks* **61**: 32–48.

[6] HUANG, G.B. and CHEN, L. (2007) Convex incremental extreme learning machine. *Neurocomputing* **70**(16-18): 3056–3062.

[7] HUANG, G.B., CHEN, L., SIEW, C.K. *et al.* (2006) Universal approximation using incremental constructive feedforward networks with random hidden nodes. *IEEE Trans. Neural Networks* **17**(4): 879–892.

[8] LIU, X., LIN, S., FANG, J. and XU, Z. (2014) Is extreme learning machine feasible? a theoretical assessment (part i). *IEEE Transactions on Neural Networks and Learning Systems* **26**(1): 7–20.

[9] LIN, S., LIU, X., FANG, J. and XU, Z. (2014) Is extreme learning machine feasible? a theoretical assessment (part ii). *IEEE Transactions on Neural Networks and Learning Systems* **26**(1): 21–34.

[10] HUANG, G.B., ZHOU, H., DING, X. and ZHANG, R. (2011) Extreme learning machine for regression and multiclass classification. *IEEE Transactions on Systems, Man, and Cybernetics, Part B (Cybernetics)* **42**(2): 513–529.

[11] CORTES, C. and VAPNIK, V. (1995) Support vector machine. *Machine learning* **20**(3): 273–297.

[12] SUYKENS, J.A. and VANDEWALLE, J. (1999) Least squares support vector machine classifiers. *Neural processing letters* **9**(3): 293–300.

[13] FERNÁNDEZ-DELGADO, M., CERNADAS, E., BARRO, S., RIBEIRO, J. and NEVES, J. (2014) Direct kernel perceptron (dkp): Ultra-fast kernel elm-based classification with non-iterative closed-form weight calculation. *Neural Networks* **50**: 60–71.

[14] HUANG, G., SONG, S., GUPTA, J.N. and WU, C. (2014) Semi-supervised and unsupervised extreme learning machines. *IEEE transactions on cybernetics* **44**(12): 2405–2417.

[15] HUANG, G.B. (2014) An insight into extreme learning machines: random neurons, random features and kernels. *Cognitive Computation* **6**(3): 376–390.

[16] HUANG, G., SONG, S. and WU, C. (2012) Orthogonal least squares algorithm for training cascade neural networks. *IEEE Transactions on Circuits and Systems I: Regular Papers* **59**(11): 2629–2637.

[17] REDDY, M.B.S. and RANA, P. (2021) Biomedical image classification using deep convolutional neural networks—overview. In *IOP Conference Series: Materials Science and Engineering* (IOP Publishing), **1022**: 012020.

[18] HUANG, P., HE, P., TIAN, S., MA, M., FENG, P., XIAO, H., MERCALDO, F. *et al.* (2022) A vit-amc network with adaptive model fusion and multiobjective optimization for interpretable laryngeal tumor grading from histopathological images. *IEEE Transactions on Medical Imaging* **42**(1): 15–28.

- [19] HUANG, P., TAN, X., ZHOU, X., LIU, S., MERCALDO, F. and SANTONE, A. (2021) Fabnet: fusion attention block and transfer learning for laryngeal cancer tumor grading in p63 ihc histopathology images. *IEEE Journal of Biomedical and Health Informatics* **26**(4): 1696–1707.
- [20] HUANG, P., ZHOU, X., HE, P., FENG, P., TIAN, S., SUN, Y., MERCALDO, F. *et al.* (2023) Interpretable laryngeal tumor grading of histopathological images via depth domain adaptive network with integration gradient cam and priori experience-guided attention. *Computers in Biology and Medicine* **154**: 106447.
- [21] CIMITILE, A., MARTINELLI, F. and MERCALDO, F. (2017) Machine learning meets ios malware: Identifying malicious applications on apple environment. In *ICISSP*: 487–492.
- [22] BACCI, A., BARTOLI, A., MARTINELLI, F., MEDVET, E. and MERCALDO, F. (2018) Detection of obfuscation techniques in android applications. In *Proceedings of the 13th International Conference on Availability, Reliability and Security*: 1–9.
- [23] CASOLARE, R., MARTINELLI, F., MERCALDO, F. and SANTONE, A. (2019) A model checking based proposal for mobile colluding attack detection. In *2019 IEEE International Conference on Big Data (Big Data)* (IEEE): 5998–6000.
- [24] DEEPA, S., DEVI, B.A. *et al.* (2011) A survey on artificial intelligence approaches for medical image classification. *Indian Journal of Science and Technology* **4**(11): 1583–1595.
- [25] ALI, M., SARWAR, A., SHARMA, V. and SURI, J. (2019) Artificial neural network based screening of cervical cancer using a hierarchical modular neural network architecture (hmna) and novel benchmark uterine cervix cancer database. *Neural Computing and Applications* **31**(7): 2979–2993.
- [26] URUSHIBARA, A., SAIDA, T., MORI, K., ISHIGURO, T., SAKAI, M., MASUOKA, S., SATOH, T. *et al.* (2021) Diagnosing uterine cervical cancer on a single t2-weighted image: comparison between deep learning versus radiologists. *European Journal of Radiology* **135**: 109471.
- [27] MOHSEN, H., EL-DAHSHAN, E.S.A., EL-HORBATY, E.S.M. and SALEM, A.B.M. (2018) Classification using deep learning neural networks for brain tumors. *Future Computing and Informatics Journal* **3**(1): 68–71.
- [28] ZIA, R., AKHTAR, P. and AZIZ, A. (2018) A new rectangular window based image cropping method for generalization of brain neoplasm classification systems. *International Journal of Imaging Systems and Technology* **28**(3): 153–162.
- [29] JAIN, M., ANDREOPOULOS, W. and STAMP, M. (2020) Convolutional neural networks and extreme learning machines for malware classification. *Journal of Computer Virology and Hacking Techniques* **16**(3): 229–244.
- [30] KRIZHEVSKY, A., SUTSKEVER, I. and HINTON, G.E. (2017) Imagenet classification with deep convolutional neural networks. *Communications of the ACM* **60**(6): 84–90.
- [31] LU, S., LU, Z. and ZHANG, Y.D. (2019) Pathological brain detection based on alexnet and transfer learning. *Journal of computational science* **30**: 41–47.
- [32] DHAR, P., DUTTA, S. and MUKHERJEE, V. (2021) Cross-wavelet assisted convolution neural network (alexnet) approach for phonocardiogram signals classification. *Biomedical Signal Processing and Control* **63**: 102142.
- [33] KUMAR M, A. and CHAKRAPANI, A. (2022) Classification of ecg signal using fft based improved alexnet classifier. *Plos one* **17**(9): e0274225.
- [34] SINGH, P., MANURE, A., SINGH, P. and MANURE, A. (2020) Introduction to tensorflow 2.0. *Learn TensorFlow 2.0: Implement Machine Learning and Deep Learning Models with Python* : 1–24.
- [35] YANG, J., SHI, R. and NI, B. (2021) Medmnet classification decathlon: A lightweight automl benchmark for medical image analysis. In *2021 IEEE 18th International Symposium on Biomedical Imaging (ISBI)* (IEEE): 191–195.
- [36] TSCHANDL, P., ROSENDAHL, C. and KITTLER, H. (2018) The ham10000 dataset, a large collection of multi-source dermatoscopic images of common pigmented skin lesions. *Scientific data* **5**(1): 1–9.
- [37] CODELLA, N., ROTEMBERG, V., TSCHANDL, P., CELEBI, M.E., DUSZA, S., GUTMAN, D., HELBA, B. *et al.* (2019) Skin lesion analysis toward melanoma detection 2018: A challenge hosted by the international skin imaging collaboration (isic). *arXiv preprint arXiv:1902.03368* .
- [38] ACEVEDO, A., MERINO, A., ALFÉREZ, S., MOLINA, Á., BOLDÚ, L. and RODELLAR, J. (2020) A dataset of microscopic peripheral blood cell images for development of automatic recognition systems. *Data in brief* **30**.